Energy & Environmental Science

ROYAL SOCIETY OF CHEMISTRY

COMMUNICATION

View Article Online
View Journal | View Issue

Check for updates

Cite this: *Energy Environ. Sci.*, 2020, **13**, 2849

Received 20th May 2020,
Accepted 13th July 2020

DOI: 10.1039/d0ee01613f

rsc.li/ees

Promoted oxygen reduction kinetics on nitrogen-doped hierarchically porous carbon by engineering proton-feeding centers†

Guangbo Chen, ‡[a] Tao Wang, ‡[b] Pan Liu, [c] Zhongquan Liao,[d] Haixia Zhong, [a] Gang Wang, [a] Panpan Zhang, [a] Minghao Yu, [a] Ehrenfried Zschech,[d] Mingwei Chen, [e] Jian Zhang *[f] and Xinliang Feng *[a]

Electrocatalytic oxygen reduction reaction (ORR) is the vital process for next-generation electrochemical energy storage and conversion technologies, *e.g.*, metal–air batteries and fuel cells. During the ORR, the O_2* and O* intermediates principally combine with protons to form OOH* and OH* species, respectively, which are the proton-coupled electron transfer processes. Unfortunately, under alkaline conditions, the protons are essentially generated from the sluggish water dissociation process, which unavoidably limits the ORR kinetics. Herein, we design and synthesize a nitrogen-doped hierarchically porous carbon with homogeneously distributed ultrafine α-MoC nanoparticles (α-MoC/NHPC) as a model electrocatalyst. Theoretical investigations unveil that α-MoC on NHPC could efficiently reduce the energy barrier of the water dissociation process to generate protons, eventually promoting the proton-coupled ORR kinetics. In a 0.1 M KOH aqueous solution, α-MoC/NHPC exhibits excellent ORR performance with a high half-wave potential of 0.88 V (*vs.* reversible hydrogen electrode), which outperforms those for NHPC and commercial Pt/C. Moreover, as the air electrode in a zinc-air battery, α-MoC/NHPC presents a large peak power density of 200.3 mW cm^{-2} and long-term stability. Thereby, our approach to engineering proton-feeding centers paves a new avenue towards the understanding of ORR kinetics and the development of high-performance ORR electrocatalysts.

Broader context

To enable large-scale commercialization of metal–air batteries, low-cost yet high-performance cathode catalysts for the sluggish oxygen reduction reaction (ORR) are urgently needed. During the ORR, the O_2* and O* intermediates generally react with protons for the formation of OOH* and OH* species, respectively. Unfortunately, under alkaline conditions, the protons are principally generated from the sluggish water dissociation process, which unavoidably limits the ORR kinetics. In this work, by engineering the water dissociation centers on a model ultrafine α-MoC nanoparticles on nitrogen-doped hierarchically porous carbon electrocatalyst, we demonstrate the significant role of the water dissociation process in proton-feeding and enhancing ORR kinetics under alkaline environment. The viable design of the proton-feeding centers and the profound understanding of the ORR kinetics in this work will open up a new approach for exploring low cost and highly-active electrocatalysts for catalytic energy conversion reactions.

The ever-increasing detrimental effects of traditional fuels on energy and environment concerns have stimulated extensive efforts for developing green and renewable energy technologies. Electrochemical oxygen reduction reaction (ORR) plays a significant role in next-generation sustainable energy storage and conversion systems, *e.g.*, metal–air batteries and fuel cells.[1–5] Up to now, platinum (Pt)-based catalysts still remain as the benchmark electrocatalysts for catalyzing the ORR.[6,7] Unfortunately, the high cost, scarcity and poor durability of Pt seriously hinder its widespread utilization in practical energy conversion systems.[8–10]

To develop efficient and earth-abundant alternatives to the Pt as ORR electrocatalysts, the profound understanding on the ORR reaction mechanism is highly desirable.[11] In alkaline

[a] *Center for Advancing Electronics Dresden (Cfaed) and Faculty of Chemistry and Food Chemistry, Technische Universität Dresden, 01062 Dresden, Germany. E-mail: xinliang.feng@tu-dresden.de*
[b] *SUNCAT Center for Interface Science and Catalysis, Department of Chemical Engineering, Stanford University, Stanford, CA 94305, USA*
[c] *School of Chemistry and Chemical Engineering, Shanghai Jiao Tong University, 200230 Shanghai, P. R. China*
[d] *Fraunhofer Institute for Ceramic, Technologies and Systems (IKTS), 01109 Dresden, Germany*
[e] *Department of Materials Science and Engineering, Johns Hopkins University, Baltimore, MD 21218, USA*
[f] *Department of Applied Chemistry, School of Applied and Natural Sciences, Northwestern Polytechnical University, Xi'an, 710129, P. R. China. E-mail: zhangjian@nwpu.edu.cn*

† Electronic supplementary information (ESI) available. See DOI: 10.1039/d0ee01613f
‡ These authors contributed equally to this work.

solutions, the ORR principally proceeds according to the ever-proposed four-electron transfer pathways: (1) $O_2(g) + * \rightarrow O_2*$; (2) $O_2* + H_2O(l) + e^- \rightarrow OOH* + OH^-$; (3) $OOH* + e^- \rightarrow O* + OH^-$; (4) $O* + H_2O(l) + e^- \rightarrow OH* + OH^-$ and (5) $OH* + e^- \rightarrow OH^- + *$, where * denotes the active site.[12] In steps (2) and (4), the O_2* and O* intermediates combine with protons to produce OOH* and OH*, respectively, which are the proton-coupled electron transfer (PCET) processes.[13] Under alkaline conditions, protons intrinsically originate from the dissociation of water molecules ($H_2O \rightarrow H* + OH*$).[14,15] The energy barrier of water dissociation in alkaline solutions undoubtedly determines the proton-feeding rates and overall ORR kinetics. Lately, nitrogen-doped hierarchically porous carbons (NHPCs) has emerged as appealing ORR catalysts alternative to the Pt owing to their low cost, earth abundance, and good electrochemical stability.[16–18] Unfortunately, the water dissociation kinetic barrier on such NHPCs is extremely high,[19,20] resulting in sluggish proton-feeding ability and low ORR activity in alkaline media (half-wave potential ($E_{1/2}$): <0.85 V *vs.* reversible hydrogen electrode (RHE)).[21–23] Recently, reported theoretical and experimental results disclose that α-MoC has superior water dissociation ability.[24,25]

In this work, by engineering the water dissociation centers on a model ultrafine α-MoC nanoparticles (NPs) on NHPC (α-MoC/NHPC) electrocatalyst, we demonstrate the significant role of water dissociation process in proton-feeding and enhancing ORR kinetics under alkaline environment. The α-MoC NPs with a diameter of ~3 nm were *in situ* synthesized on NHPC by pyrolyzing a mixture of NaCl and phosphomolybdic acid/zeolitic imidazolate framework-8 (Mo12/ZIF-8) precursors. Density functional theory (DFT) calculations reveal that the α-MoC NPs in α-MoC/NHPC could effectively reduce the kinetic energy barrier of water dissociation and thereby provide plentiful protons for accelerating the PCET steps, eventually promoting the ORR kinetics in alkaline solutions (Scheme 1). As a result, α-MoC/NHPC electrocatalyst exhibits excellent ORR activity with an $E_{1/2}$ of as high as 0.88 V in a 0.1 M KOH aqueous solution, which surpasses those values for NHPC ($E_{1/2} = 0.84$ V), Pt/C catalyst ($E_{1/2} = 0.85$ V) and previously reported metal-free electrocatalysts. Moreover, as the air electrode in an as-assembled Zn–air battery, α-MoC/NHPC demonstrates an extremely high peak power density of 200.3 mW cm^{-2}, which is much higher than that for Pt/C (154.1 mW cm^{-2}).

As schematically illustrated in Fig. 1a, α-MoC/NHPC electrocatalyst was synthesized by using a NaCl-assisted pyrolysis of Mo12/ZIF-8 precursors. First, the Mo12/ZIF-8 was prepared *via* co-precipitation of $Zn(NO_3)_2{\cdot}6H_2O$ (2.97 g), 2-methylimidazole (3.28 g) in a methanol solution (160 mL) containing phosphomolybdic acid (Mo12, 60 mg) at room temperature for 24 h (Fig. S1 and S2, ESI†). Second, the achieved Mo12/ZIF-8 (100 mg) was physically mixed with NaCl (35 mg) and then heated at 900 °C for 2 hours under nitrogen atmosphere. Here, NaCl served as templates and intercalating agents for the formation of hierarchically porous carbon nanostructures.[26] After washing and drying, α-MoC/NHPC with an α-MoC loading amount of 5.0 wt% was obtained. For comparison, α-MoC/NHPCs with different loading amounts of α-MoC (α-MoC: 1.4, 2.4, 5.0, 6.8 and 8.1 wt%) while with a similar NP size (~3 nm) were fabricated by changing the dosage of Mo12 (Fig. S3–S8, ESI†). Moreover, NHPC was prepared without the utilization of Mo12 (Fig. S9, ESI†).

The morphologies of resultant α-MoC/NHPC were firstly investigated using transmission electron microscopy (TEM). As shown in Fig. 1b and c, the α-MoC NPs with a mean diameter of 3.0 nm are uniformly decorated on the NHPC. The high-angle annular dark field-scanning transmission electron microscopy

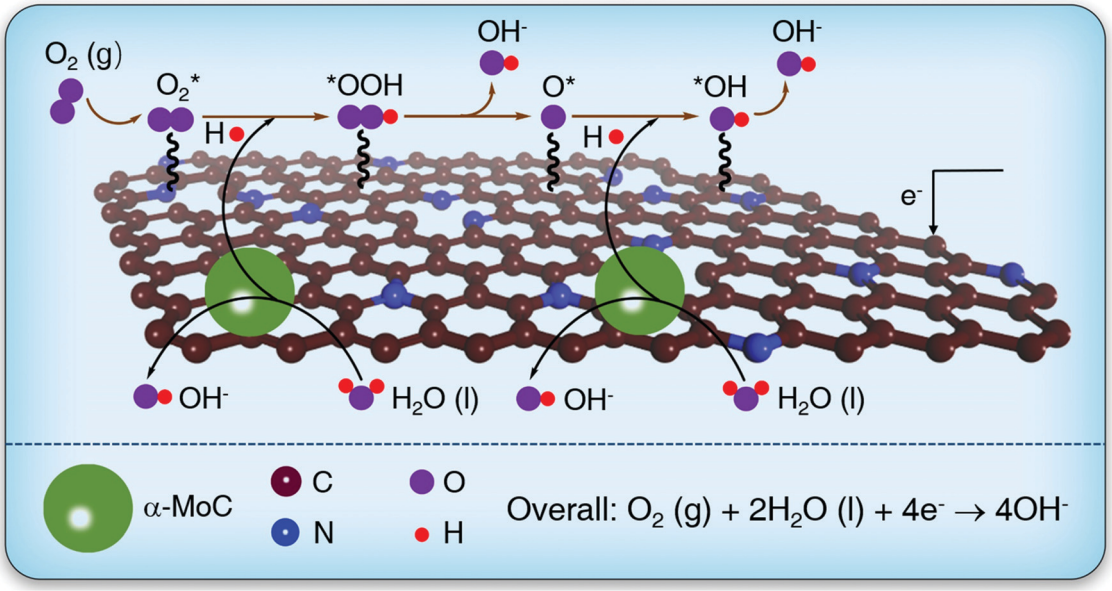

Scheme 1 Schematic illustration for water dissociation step and the subsequent elementary processes for ORR in alkaline solutions over an α-MoC/NHPC electrocatalyst.

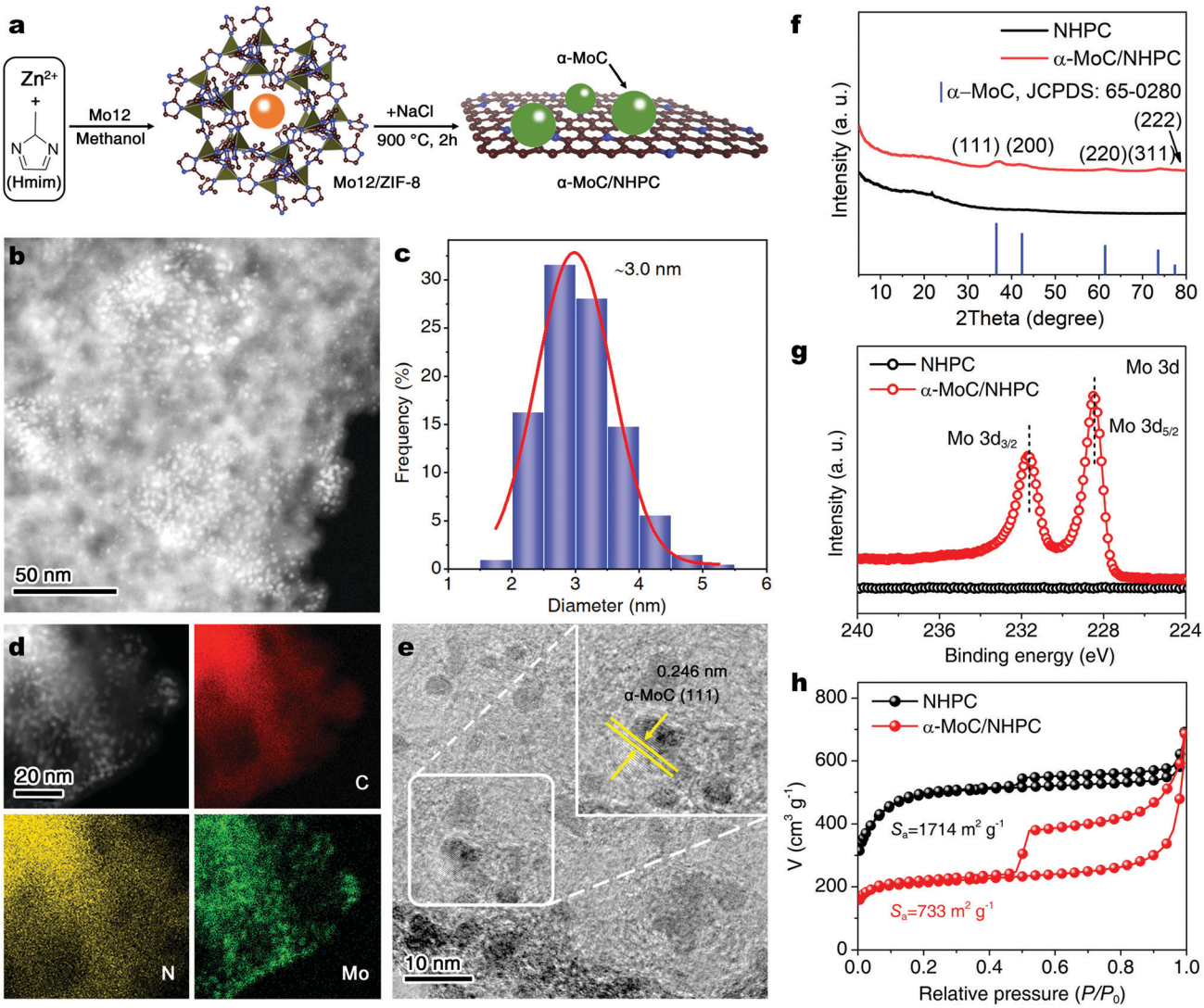

Fig. 1 (a) Schematic illustration of the synthesis of α-MoC/NHPC. (b) HAADF-STEM image of α-MoC/NHPC and (c) the corresponding α-MoC NPs size distribution. (d) Elemental mapping images showing the distribution of C (red), N (yellow), and Mo (green) elements. (e) HRTEM image of α-MoC/NHPC. (f) XRD patterns, (g) high-resolution Mo 3d XPS spectra, (h) N_2 adsorption/desorption isotherms of NHPC and α-MoC/NHPC.

(HAADF-STEM) and corresponding energy-dispersive X-ray spectroscopy (EDX) elemental mapping images reveal the distributions of C, N and Mo elements over the α-MoC/NHPC (Fig. 1d). The NPs show a homogeneous distribution of Mo element. High-resolution TEM (HRTEM) image displays clear lattice fringes with an interplanar spacing of 0.246 nm, corresponding to the (111) lattice plane of α-MoC (Fig. 1e and Fig. S10, ESI†). The crystalline structure of the achieved α-MoC/NHPC was further confirmed by X-ray diffraction (XRD) analysis. As disclosed in Fig. 1f, the diffraction peaks at 36.4°, 42.3°, 61.3°, 73.4° and 77.3° are indexed to the characteristic (111), (200), (220), (311) and (222) facets of the α-MoC (JCPDS No. 65-0280), respectively.[24,25] The Raman spectrum of α-MoC/NHPC shows two peaks at 1350 and 1590 cm^{-1} (Fig. S11, ESI†), which are assigned to disordered sp^3 carbon (D band) and graphitic sp^2 carbon (G band) of NHPC, respectively.[27]

To gain insights into the surface chemical composition and elemental bonding configurations of the achieved α-MoC/NHPC and NHPC, X-ray photoelectron spectroscopy (XPS) analyses were conducted. As illustrated in Fig. S12 (ESI†), the survey spectrum of α-MoC/NHPC confirms the presence of C, N and Mo. High-resolution N 1s spectra of α-MoC/NHPC and NHPC can be well fitted into four characteristic peaks of pyridinic N (398.5 eV), pyrrolic N (400.3 eV), graphitic N (401.2 eV) and oxidized N (402.7 eV)[28,29] (Fig. S13, ESI†). The pyridinic N content in α-MoC/NHPC is approximately 4.8 at%, which is lower than 5.5 at% for NHPC (Table S1, ESI†). In the high-resolution Mo 3d XPS spectrum of α-MoC/NHPC, the binding energies of Mo $3d_{5/2}$ and Mo $3d_{3/2}$ located at 228.4 eV and 231.6 eV are attributed to Mo^{2+} (Fig. 1g).[24,25] The α-MoC content in α-MoC/NHPC was determined to be 5.0 wt% based on the inductively coupled plasma mass spectrometry (ICP-MS) analysis. The elemental analysis results reveal that the C and N contents in α-MoC/NHPC are 81.6 at% and 6.7 at%, respectively. (Table S1, ESI†). Next, N_2 sorption analysis was carried

out to assess the textural properties of the achieved NHPC and α-MoC/NHPC. The Barrett–Emmett–Teller (BET) surface area of α-MoC/NHPC was measured to be 733 $m^2 g^{-1}$, which was much smaller than 1714 $m^2 g^{-1}$ for NHPC (Fig. 1h). A detailed pore structure analysis reveals that α-MoC/NHPC shows a less microporous/mesoporous structure in comparison with that of NHPC, attributable to the partial blockage of pores by the α-MoC NPs (Fig. S14, ESI†). The specific micropore and mesopore surface areas of α-MoC/NHPC are 526 $m^2 g^{-1}$ and 143 $m^2 g^{-1}$, respectively.

The electrocatalytic ORR performances of α-MoC/NHPC were investigated by linear sweep voltammetry (LSV) in an O_2-saturated 0.1 M KOH aqueous solution. By contrast, a commercial Pt/C (20% Pt, Fuelcellstore) and NHPC were also evaluated. All potentials were referenced to the RHE. As shown in Fig. 2a, the α-MoC/NHPC demonstrated excellent ORR activity with an onset potential of 0.98 V. The $E_{1/2}$ of α-MoC/NHPC reached 0.88 V, which was higher than those for Pt/C (0.85 V), NHPC (0.84 V) and the previously reported ORR electrocatalysts, such as, nitrogen-doped three-dimensional graphene nanoribbon networks (N-GRW, $E_{1/2}$ = 0.84 V),[30] three-dimensional nitrogen and phosphorus co-doped mesoporous carbon (NPMC, $E_{1/2}$ = 0.85),[31] single-atom Co supported by porous nitrogen-doped carbon nanospheres (Co-ISAS/p-CN, $E_{1/2}$ = 0.838 V),[32] single atomic Cu in ultrathin nitrogenated carbon nanosheets (Cu–N–C, $E_{1/2}$ = 0.85 V),[33] atomically dispersed Fe atoms anchored on porous N- and S-codoped carbon framework (Fe SAs/NSC, $E_{1/2}$ = 0.87 V).[34] Meanwhile, the kinetic current density (J_k) of α-MoC/NHPC was up to 33.8 mA cm^{-2} at 0.80 V, which was considerably larger than those of NHPC (17.8 mA cm^{-2}) and Pt/C (21.4 mA cm^{-2}) (Fig. 2b and Table S2, ESI†). The corresponding Tafel slope of α-MoC/NHPC was determined to be ~47.8 mV $decade^{-1}$, which was much lower than 83.2 mV $decade^{-1}$ for Pt/C and 56.1 mV $decade^{-1}$ for NHPC, demonstrating an accelerated ORR kinetics on α-MoC/NHPC electrocatalyst (Fig. 2c). Moreover, the α-MoC/NHPC electrocatalyst also reveals superior selectivity toward OH^- formation *via* a four-electron dominant transfer pathway and superb stability (Fig. S15–S19, ESI†).

In order to reveal the key role of α-MoC NPs during the alkaline ORR process, we investigated the ORR performance of a series of α-MoC/NHPCs with different α-MoC loading contents (1.4, 2.4, 5.0, 6.8 and 8.1 wt%) in a 0.1 M KOH aqueous solution. As shown in Fig. S20 (ESI†) and Fig. 2d, the $E_{1/2}$ of α-MoC/NHPCs increased accompanied by larger α-MoC contents. When the weight content of α-MoC was 5.0 wt%, the α-MoC/NHPC showed the highest $E_{1/2}$ (0.88 V). Then, the $E_{1/2}$ of α-MoC/NHPC decreased when increasing the α-MoC content (6.8 wt%, 0.85 V), which was probably due to the blockage of the intrinsic ORR active site of NHPC by the high coverage of α-MoC NPs, as indicated by the reduced electrochemically active surface area (ECSA) and ORR kinetics (Fig. S21 and S22, ESI†).

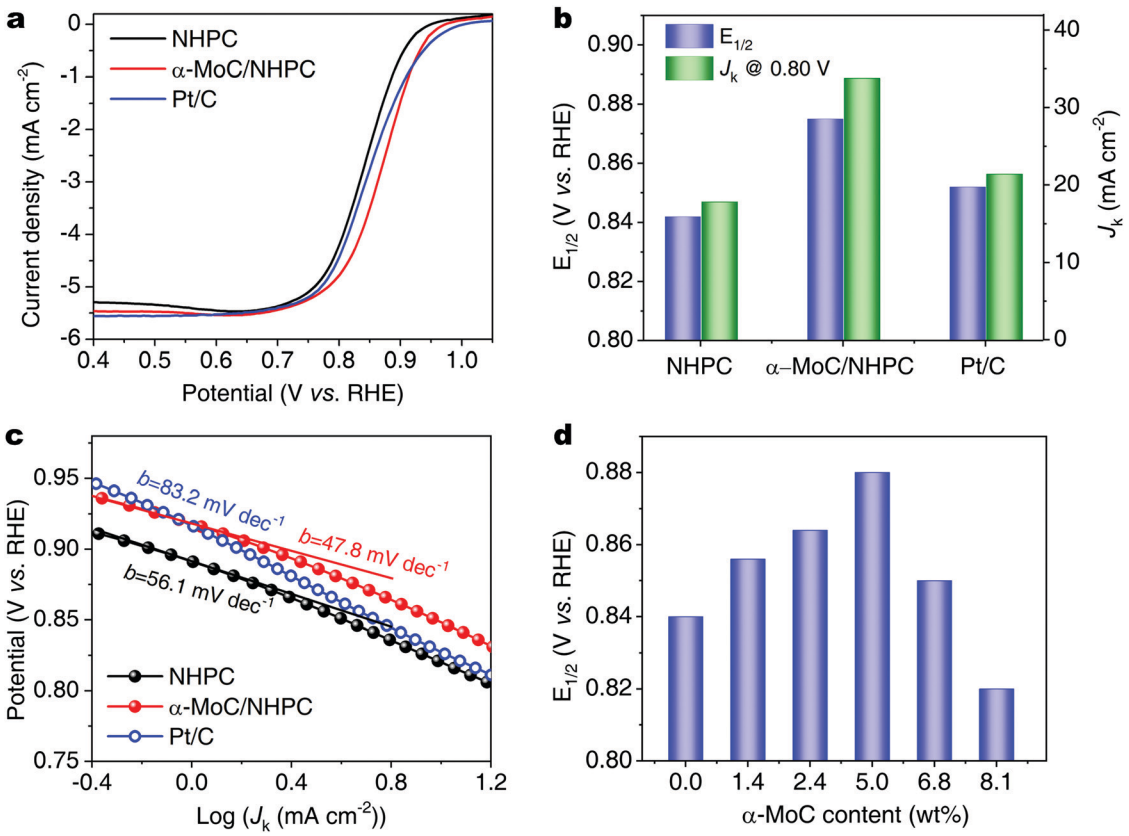

Fig. 2 (a) ORR polarization curves, (b) J_k at 0.80 V and $E_{1/2}$, and (c) corresponding Tafel slopes of NHPC, α-MoC/NHPC and Pt/C. (d) $E_{1/2}$ of α-MoC/NHPCs with different α-MoC contents.

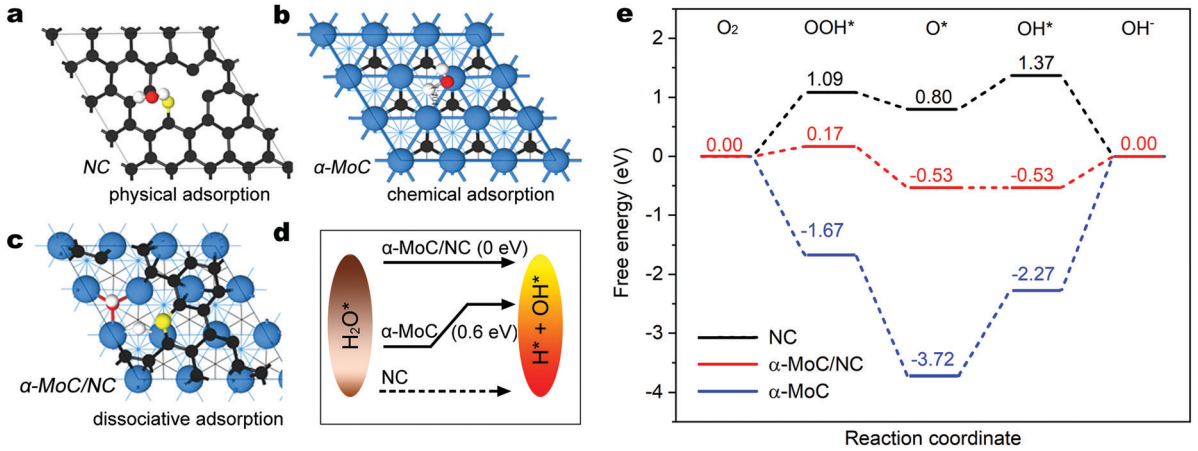

Fig. 3 Adsorption configurations of water on (a) NC, (b) α-MoC(111) and (c) α-MoC/NC surfaces. (d) Schematic energy diagrams for water dissociation and (e) free energy diagrams for ORR on NC, α-MoC(111) and α-MoC/NC catalysts at the overpotential of 0 V.

To further elucidate the fundamental mechanism of the outstanding ORR activity of α-MoC/NHPC, the kinetic energy barrier of the water dissociation step and the subsequent ORR elementary processes were studied using DFT calculations based on the as-built electrocatalyst models including nitrogen doped carbon (NC), α-MoC(111) and α-MoC/NC (Fig. S23, ESI†). Fig. 3a–c present the water adsorption configurations on the as-constructed models. As illustrated in Fig. 3a, H_2O can be only physically adsorbed on the NC and is hard to be dissociated, indicating an extremely sluggish water dissociation kinetics for the generation of protons.[35] On the α-MoC(111), water is chemically adsorbed and can be dissociated into H* and OH* with an energy barrier of only 0.6 eV (Fig. 3b and Fig. S24, ESI†), suggesting an excellent water dissociation kinetics, which is consistent with the reported results.[25] Surprisingly, water molecule demonstrates dissociative adsorption on the α-MoC/NC that can be spontaneously dissociated for the formation of H* and OH*,[36] implying a superior property of water dissociation for proton feeding in comparison with those on NC and α-MoC (Fig. 3c and d). Fig. 3e displays the free energy diagram for the

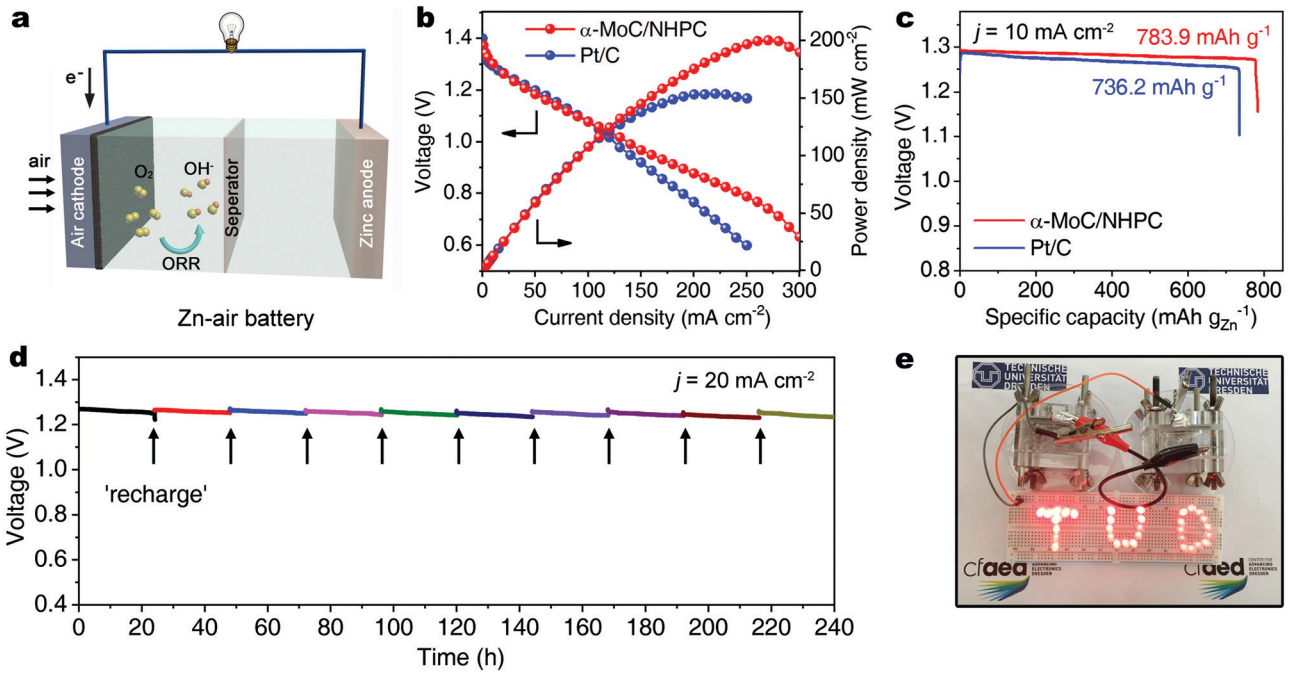

Fig. 4 (a) Schematic illustration of an as-assembled Zn–air battery. (b) Discharge polarization curves and corresponding power density plots of the primary Zn–air batteries using α-MoC/NHPC and Pt/C as air electrode, respectively. (c) Long-time galvanostatic discharge curves of a Zn–air battery with α-MoC/NHPC as cathode catalyst until complete consumption of Zn anode. The specific capacity was normalized to the mass of consumed Zn. (d) Discharge plot of the Zn–air battery with α-MoC/NHPC as cathode catalyst by replenishing Zn anode and electrolyte. (e) Photograph of red LEDs in series powered by two tandem Zn–air batteries.

elementary steps of ORR at the overpotential of 0 V. For α-MoC, the formation of OOH* and O* species are all exothermic and downhill, evidencing thermodynamically favorable processes (Fig. S25, ESI†). However, the reduction of O* to OH* and the release of OH from the active sites on α-MoC are uphill processes with energy barriers of 1.45 eV and 2.27 eV, respectively, indicating that the pure α-MoC can be easily poisoned by O* and OH* intermediates that block the ORR kinetics. On NC and α-MoC/NC, the C atoms neighboring to N in NC are the real active site due to they demonstrate the most stable adsorption for reaction intermediates (OOH*, O* and OH*), according to the systematic DFT calculations (Fig. S26 and S27, ESI†). On NC, the energy barriers for O* to OOH* and O* to OH* are as high as 1.09 eV and 0.57 eV, respectively, which undoubtedly limit the overall ORR kinetics. Notably, on α-MoC/NC, the energy barriers for O* to OOH* and O* to OH* considerably decrease to 0.17 eV and 0.00 eV, respectively, indicating promoted PECT processes, as a result of an accelerated water dissociation kinetics for proton feeding.[37]

To investigate the practical applicability of the as-developed α-MoC/NHPC electrocatalyst in energy devices, a primary Zn–air battery was assembled utilizing α-MoC/NHPC as the oxygen electrocatalyst on air electrode in a 6.0 M KOH electrolyte containing 0.2 M $Zn(OAc)_2$ (Fig. 4a).[38] As depicted in Fig. S28 (ESI†), the open-circuit voltage of the α-MoC/NHPC was 1.44 V. The maximum power density of α-MoC/NHPC was up to 200.3 mW cm^{-2} (Fig. 4b), which substantially exceeded 154.1 mW cm^{-2} for Pt/C and those for the previously reported ORR electrocatalysts, *e.g.*, N-GRW (65 mW cm^{-2}),[30] NMPC (55 mW cm^{-2}),[31] metal-free mesoporous N-doped carbons (192.7 mW cm^{-2}),[39] Mn/Fe-HIB-MOF (195 mW cm^{-2}),[40] MnO/Co in porous graphitic carbon (172 mW cm^{-2})[41] and PdMo bimetallene (154.2 mW cm^{-2})[42] (Table S3, ESI†). Meanwhile, the α-MoC/NHPC catalyst-based Zn–air battery delivered a specific capacity of 783.9 mA h g_{Zn}^{-1} at 10 mA cm^{-2}, corresponding to a ~95.6% utilization efficiency of the theoretical capacity (~820 mA h g_{Zn}^{-1}) (Fig. 4c). Furthermore, α-MoC/NHPC electrocatalyst could stably work in a mechanically rechargeable battery by only refueling the consumed zinc anode and electrolyte at the end of each discharge. No noticeable degradation was observed after 10 cycles over a period of 240 hours at a current density of 20 mA cm^{-2}, highlighting the superior durability of α-MoC/NHPC electrocatalyst (Fig. 4d). Such two tandem Zn–air batteries steadily lighted up red light-emitting diodes (LEDs) in series more than ten days, promising their potential utilization for powering electronic devices (Fig. 4e).

Conclusions

In conclusion, we demonstrate that the water dissociation plays an essential role for proton-feeding and eventually accelerating the ORR kinetics in alkaline solutions by engineering the water dissociation centers on a model α-MoC/NHPC electrocatalyst. As a result, the as-constructed α-MoC/NHPC exhibits excellent ORR activity in alkaline solutions, which is superior to those of the noble metal Pt/C and the state-of-art noble metal-free electrocatalysts. Therefore, the viable design of the proton-feeding centers and the profound understanding of the ORR kinetics not only provide a promising alternative ORR catalyst to the Pt, but also open up a new window for exploring low cost and high-activity electrocatalysts for energy-conversion-related catalytic reactions including oxygen reduction, CO_2 reduction, water splitting, and nitrogen reduction reaction, *etc.*

Author contributions

G. C., J. Z. and X. F. conceived the idea, designed the experiments and wrote the paper. G. C. synthesized the materials. G. C. and H. Z. conducted the electrocatalytic tests and analyzed the data. T. W. did the DFT calculations. P. L., Z. L., E. Z. and M. C performed the TEM, HRTEM and HAADF-STEM measurements. P. Z. performed the SEM characterizations. G. W. and M. Y. rendered helpful discussions. All authors discussed the results and commented on the manuscript.

Conflicts of interest

There are no conflicts to declare.

Acknowledgements

This work was financially supported by the European Research Council (ERC) under the European Union's Horizon 2020 research and innovation programme (grant agreement No. 819698 and GrapheneCore3 881603), Deutsche Forschungsgemeinschaft (MXOSMOPED project) and Coordination Networks: Building Blocks for Functional Systems (SPP 1928, COORNET). We acknowledge the Center for Advancing Electronics Dresden (Cfaed), the Dresden Center for Nanoanalysis (DCN) at TU Dresden. G. Chen thanks China Scholarship Council for the financial support. Prof. J. Zhang acknowledges funding support from Shannxi National Science Foundation (No. 2020JQ-141) and the Fundamental Research Funds for the Central Universities (No. 310201911cx028).

References

1 M. Shao, Q. Chang, J.-P. Dodelet and R. Chenitz, *Chem. Rev.*, 2016, **116**, 3594–3657.
2 Y. Jiang, Y.-P. Deng, J. Fu, D. U. Lee, R. Liang, Z. P. Cano, Y. Liu, Z. Bai, S. Hwang, L. Yang, D. Su, W. Chu and Z. Chen, *Adv. Energy Mater.*, 2018, **8**, 1702900.
3 G. Chen, P. Liu, Z. Liao, F. Sun, Y. He, H. Zhong, T. Zhang, E. Zschech, M. Chen, G. Wu, J. Zhang and X. Feng, *Adv. Mater.*, 2020, **32**, 1907399.
4 Y.-P. Deng, Y. Jiang, R. Liang, S.-J. Zhang, D. Luo, Y. Hu, X. Wang, J.-T. Li, A. Yu and Z. Chen, *Nat. Commun.*, 2020, **11**, 1952.
5 H.-F. Wang, L. Chen, H. Pang, S. Kaskel and Q. Xu, *Chem. Soc. Rev.*, 2020, **49**, 1414–1448.
6 X. Huang, Z. Zhao, L. Cao, Y. Chen, E. Zhu, Z. Lin, M. Li, A. Yan, A. Zettl, Y. M. Wang, X. Duan, T. Mueller and Y. Huang, *Science*, 2015, **348**, 1230–1234.

7 M. Liu, L. Wang, K. Zhao, S. Shi, Q. Shao, L. Zhang, X. Sun, Y. Zhao and J. Zhang, *Energy Environ. Sci.*, 2019, **12**, 2890–2923.
8 M. K. Debe, *Nature*, 2012, **486**, 43.
9 Y.-P. Deng, R. Liang, G. Jiang, Y. Jiang, A. Yu and Z. Chen, *ACS Energy Lett.*, 2020, **5**, 1665–1675.
10 G. Chen, T. Wang, J. Zhang, P. Liu, H. Sun, X. Zhuang, M. Chen and X. Feng, *Adv. Mater.*, 2018, **30**, 1706279.
11 H. Jiang, J. Gu, X. Zheng, M. Liu, X. Qiu, L. Wang, W. Li, Z. Chen, X. Ji and J. Li, *Energy Environ. Sci.*, 2019, **12**, 322–333.
12 Y. Jiao, Y. Zheng, M. Jaroniec and S. Z. Qiao, *Chem. Soc. Rev.*, 2015, **44**, 2060–2086.
13 Z. W. Seh, J. Kibsgaard, C. F. Dickens, I. Chorkendorff, J. K. Nørskov and T. F. Jaramillo, *Science*, 2017, **355**, eaad4998.
14 Y. Zheng, Y. Jiao, A. Vasileff and S.-Z. Qiao, *Angew. Chem., Int. Ed.*, 2018, **57**, 7568–7579.
15 N. Mahmood, Y. Yao, J.-W. Zhang, L. Pan, X. Zhang and J.-J. Zou, *Adv. Sci.*, 2018, **5**, 1700464.
16 X. Liu and L. Dai, *Nat. Rev. Mater.*, 2016, **1**, 16064.
17 J. Zhang, G. Chen, K. Müllen and X. Feng, *Adv. Mater.*, 2018, **30**, 1800528.
18 C. Zhu, H. Li, S. Fu, D. Du and Y. Lin, *Chem. Soc. Rev.*, 2016, **45**, 517–531.
19 C. Lu, D. Tranca, J. Zhang, F. N. Rodríguez Hernández, Y. Su, X. Zhuang, F. Zhang, G. Seifert and X. Feng, *ACS Nano*, 2017, **11**, 3933–3942.
20 W. Han, L. Chen, B. Ma, J. Wang, W. Song, X. Fan, Y. Li, F. Zhang and W. Peng, *J. Mater. Chem. A*, 2019, **7**, 4734–4743.
21 R. Paul, L. Zhu, H. Chen, J. Qu and L. Dai, *Adv. Mater.*, 2019, **31**, 1806403.
22 L. Yang, J. Shui, L. Du, Y. Shao, J. Liu, L. Dai and Z. Hu, *Adv. Mater.*, 2019, **31**, 1804799.
23 K. Gao, B. Wang, L. Tao, B. V. Cunning, Z. Zhang, S. Wang, R. S. Ruoff and L. Qu, *Adv. Mater.*, 2019, **31**, 1805121.
24 S. Yao, X. Zhang, W. Zhou, R. Gao, W. Xu, Y. Ye, L. Lin, X. Wen, P. Liu, B. Chen, E. Crumlin, J. Guo, Z. Zuo, W. Li, J. Xie, L. Lu, C. J. Kiely, L. Gu, C. Shi, J. A. Rodriguez and D. Ma, *Science*, 2017, **357**, 389–393.
25 L. Lin, W. Zhou, R. Gao, S. Yao, X. Zhang, W. Xu, S. Zheng, Z. Jiang, Q. Yu, Y.-W. Li, C. Shi, X.-D. Wen and D. Ma, *Nature*, 2017, **544**, 80.
26 N. Fechler, T.-P. Fellinger and M. Antonietti, *Adv. Mater.*, 2013, **25**, 75–79.
27 L. Tao, M. Qiao, R. Jin, Y. Li, Z. Xiao, Y. Wang, N. Zhang, C. Xie, Q. He and D. Jiang, *Angew. Chem., Int. Ed.*, 2019, **58**, 1019–1024.
28 H.-W. Liang, X. Zhuang, S. Brüller, X. Feng and K. Müllen, *Nat. Commun.*, 2014, **5**, 4973.
29 N. Agarwal, S. J. Freakley, R. U. McVicker, S. M. Althahban, N. Dimitratos, Q. He, D. J. Morgan, R. L. Jenkins, D. J. Willock, S. H. Taylor, C. J. Kiely and G. J. Hutchings, *Science*, 2017, **358**, 223–227.
30 H. B. Yang, J. Miao, S.-F. Hung, J. Chen, H. B. Tao, X. Wang, L. Zhang, R. Chen, J. Gao, H. M. Chen, L. Dai and B. Liu, *Sci. Adv.*, 2016, **2**, 1501122.
31 J. Zhang, Z. Zhao, Z. Xia and L. Dai, *Nat. Nanotechnol.*, 2015, **10**, 444.
32 A. Han, W. Chen, S. Zhang, M. Zhang, Y. Han, J. Zhang, S. Ji, L. Zheng, Y. Wang, L. Gu, C. Chen, Q. Peng, D. Wang and Y. Li, *Adv. Mater.*, 2018, **30**, 1706508.
33 F. Li, G.-F. Han, H.-J. Noh, S.-J. Kim, Y. Lu, H. Y. Jeong, Z. Fu and J.-B. Baek, *Energy Environ. Sci.*, 2018, **11**, 2263–2269.
34 J. Zhang, Y. Zhao, C. Chen, Y.-C. Huang, C.-L. Dong, C.-J. Chen, R.-S. Liu, C. Wang, K. Yan, Y. Li and G. Wang, *J. Am. Chem. Soc.*, 2019, **141**, 20118–20126.
35 M. A. Henderson, *Surf. Sci. Rep.*, 2002, **46**, 1–308.
36 P. J. Feibelman, *Science*, 2002, **295**, 99–102.
37 Q. Yang, Y. Jia, F. Wei, L. Zhuang, D. Yang, J. Liu, X. Wang, S. Lin, P. Yuan and X. Yao, *Angew. Chem., Int. Ed.*, 2020, **59**, 6122–6127.
38 Y. Li, M. Gong, Y. Liang, J. Feng, J.-E. Kim, H. Wang, G. Hong, B. Zhang and H. Dai, *Nat. Commun.*, 2013, **4**, 1805.
39 X. Peng, L. Zhang, Z. Chen, L. Zhong, D. Zhao, X. Chi, X. Zhao, L. Li, X. Lu, K. Leng, C. Liu, W. Liu, W. Tang and K. P. Loh, *Adv. Mater.*, 2019, **31**, 1900341.
40 S. S. Shinde, C. H. Lee, J.-Y. Jung, N. K. Wagh, S.-H. Kim, D.-H. Kim, C. Lin, S. U. Lee and J.-H. Lee, *Energy Environ. Sci.*, 2019, **12**, 727–738.
41 X. F. Lu, Y. Chen, S. Wang, S. Gao and X. W. Lou, *Adv. Mater.*, 2019, **31**, 1902339.
42 M. Luo, Z. Zhao, Y. Zhang, Y. Sun, Y. Xing, F. Lv, Y. Yang, X. Zhang, S. Hwang, Y. Qin, J.-Y. Ma, F. Lin, D. Su, G. Lu and S. Guo, *Nature*, 2019, **574**, 81–85.